AIAA Guidance, Navigation, and Control Conference and Exhibit
15 - 18 August 2005, San Francisco, California

AIAA 2005-6176

Solar Sail Trajectory Optimization for Intercepting, Impacting, and Deflecting Near-Earth Asteroids

Bernd Dachwald*
German Aerospace Center (DLR), 51170 Cologne, Germany
Bong Wie†
Arizona State University, Tempe, AZ 85287, USA

A fictional asteroid mitigation problem posed by AIAA assumes that a 200 m near-Earth asteroid (NEA), detected on 04 July 2004 and designated as 2004 WR, will impact the Earth on 14 January 2015. Adopting this exemplary scenario, we show that solar sail spacecraft that impact the asteroid with very high velocity are a realistic near-term option for mitigating the impact threat from NEAs. The proposed mission requires several Kinetic Energy Interceptor (KEI) solar sail spacecraft. Each sailcraft consists of a 160 m × 160 m, 168 kg solar sail and a 150 kg impactor. Because of their large ΔV-capability, solar sailcraft with a characteristic acceleration of 0.5 mm/s^2 can achieve an orbit that is retrograde to the target orbit within less than about 4.5 years. Prior to impacting 2004 WR at its perihelion of about 0.75 AU, each impactor is to be separated from its solar sail. With a relative impact velocity of about 81 km/s, each impactor will cause a conservatively estimated Δv of about 0.35 cm/s in the trajectory of the target asteroid, largely due to the impulsive effect of material ejected from the newly formed crater. The deflection caused by a single impactor will increase the Earth-miss distance by about 0.7 Earth radii. Several sailcraft will therefore be required for consecutive impacts to increase the total Earth-miss distance to a safe value. In this paper, we elaborate a potential mission scenario and investigate trade-offs between different mission parameters, e.g. characteristic acceleration, sail temperature limit, hyperbolic excess energy for interplanetary insertion, and optical solar sail degradation.

I. Introduction

Near-Earth objects (NEOs) are asteroids and short-period comets with orbits that intersect or pass near the orbit of Earth (perihelion $r_p \leq 1.3$ AU). About 794 NEAs with an absolute magnitude H ≤ 18 (diameter $d \gtrsim 1$ km) are currently (July 05) known,[1] but the entire population contains perhaps more than 1 000 objects of this size.[2] All NEAs with an Earth Minimum Orbit Intersection Distance (MOID) ≤ 0.05 AU and H ≤ 22 ($d \gtrsim 200$ m) are termed Potentially Hazardous Asteroids (PHAs). There are currently 663 known PHAs, 7 of them with H ≤ 15 ($d \gtrsim 5$ km).[1] They pose a significant hazard to human civilization and to life on Earth. It is today widely accepted that NEO impacts have caused at least one mass extinction (65 million years ago at the Cretaceous/Tertiary boundary), and they are suspected to have caused several global catastrophes before.[3] A 2 km object is capable of causing catastrophic alteration of the global ecosystem. Ocean impacts of even smaller objects are of some concern because the destructive potential caused by the resulting tsunamis may be above that from a land impact. Even objects that do not intersect Earth's orbit may evolve into Earth-crossers, since their orbits are chaotic, having a relatively short dynamical lifetime[4,5] ($\sim 10^7$ years). Although this paper is about a fictional scenario, one day it might become necessary to prevent a specific object from impacting the Earth by nudging it out of its orbit. The probability of major impacts with severe effects for humanity is low but not zero. This paper presents a realistic near-term solution to mitigate this threat.

*Scientist, Institute of Space Simulation, Linder Hoehe, bernd.dachwald@dlr.de, +49-2203-601 3001, Member AIAA.
†Professor, Dept. of Mechanical & Aerospace Engineering, bong.wie@asu.edu, +1-480-965 8674, Associate Fellow AIAA.

II. Mission Scenario

A fictional asteroid mitigation problem was created by AIAA for the 2004/2005 AIAA Foundation Undergraduate Team Space Design Competition: on 04 July 2004, NASA/JPL's Near Earth Asteroid Tracking (NEAT) camera at the Maui Space Surveillance Site discovered an Apollo asteroid with an estimated diameter of 0.205 km designated 2004WR. This asteroid has been assigned a Torino Impact Scale rating of 9.0 on the basis of subsequent observations that indicate a 95% probability that 2004WR will impact the Earth. The expected impact will occur in the Southern Hemisphere on 14 January 2015 causing catastrophic damage throughout the Pacific region. The mission task is to design a space system that can rendezvous with 2004WR in a timely manner, inspect it, and remove the hazard to Earth by changing its orbit and/or destroying it. The classical orbital elements of 2004WR are given in the J2000 heliocentric ecliptic reference frame as follows:

$$\begin{aligned} \text{Epoch} &= 53200\,\text{TDB}\ (14\,\text{July}\,2004) \\ a &= 2.15374076\,\text{AU} \\ e &= 0.649820926 \\ i &= 11.6660258\,\text{deg} \\ \omega &= 66.2021796\,\text{deg} \\ \Omega &= 114.4749665\,\text{deg} \\ M &= 229.8987151\,\text{deg} \end{aligned}$$

It was further assumed that 2004WR is an S-class (stony-silicate) asteroid with a density of $2\,720\,\text{kg/m}^3$ and that its estimated mass is 1.1×10^{10} kg.

The proposed mission scenario employs a solar sail to deliver impactors to an orbit retrograde to the asteroid's orbit, from where they impact the target with very high kinetic energy. The use of solar sails to achieve impacts from retrograde orbits was first proposed (and elaborated in a more general way) by McInnes in Ref. 6. The proposed mission scenario comprises three phases (Fig. 1): (1) a spiralling-in phase, (2) an orbit cranking phase to an orbit retrograde to the asteroid's one, and (3) a final retrograde orbit phase prior to impacting the target asteroid at its perihelion with maximum efficiency.

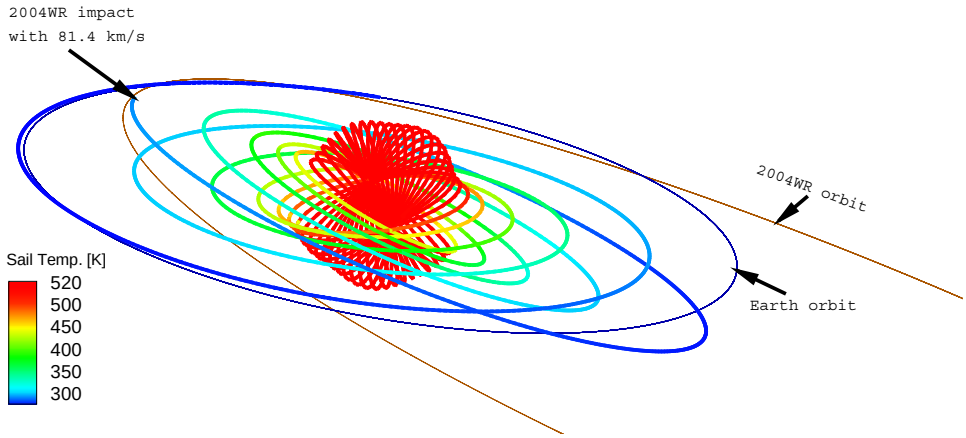

Figure 1. Proposed mission scenario

A head-on collision yields an impact velocity of more than 80 km/s, which is much higher than the typical impact velocity of about 10 km/s of conventional missions such as NASA's Deep Impact mission[7,8] or ESA's Don Quijote mission.[9] The impactor is to be separated from the solar sail prior to impacting the target asteroid, because of the extremely demanding terminal guidance and targeting requirements (the accuracy of the impactor trajectory must be much better than 100 m at a relative velocity of more than 80 km/s). For the present scenario, several KEI sailcraft will be required to increase the Earth-miss distance to a safe value. For larger asteroids, the impactor may not have to be separated from the solar sail, but the complete solar sail spacecraft could be designed to impact, thereby increasing the impacting mass and thus the resulting

Δv. The critical technologies required for the proposed mission include: (1) deployment and control of a 160 m × 160 m solar sail, (2) development of a solar sail and a micro-spacecraft bus that is able to withstand the extreme space environment at less than only 0.25 AU from the sun, (3) autonomous precision navigation, terminal guidance and targeting, and (4) accurate impact-crater ejecta modeling and Δv prediction. A 160 m × 160 m solar sail is currently not available. However, a 20 m × 20 m solar sail structure was already deployed on ground in a simulated gravity-free environment at DLR in December 1999, a 40 m × 40 m solar sail is being developed by NASA and industries for a possible flight validation experiment within 10 years, and thus a 160 m × 160 m solar sail is expected to be available within about 20 years of a sharply pursued technology development program.

III. Solar Sail Force Model

For the description of the solar radiation pressure (SRP) force exerted on a solar sail, it is convenient to introduce two unit vectors. The first one is the sail normal vector $\boldsymbol{n}$, which is perpendicular to the sail surface and always directed away from the sun. In the orbit frame[a] $\mathcal{O}$, its direction, which describes the sail attitude, is expressed by the pitch angle α and the clock angle δ (Fig. 2). The second unit vector is the thrust unit vector $\boldsymbol{m}$, which points along the direction of the SRP force. Its direction is described likewise by the cone angle θ and the clock angle δ.

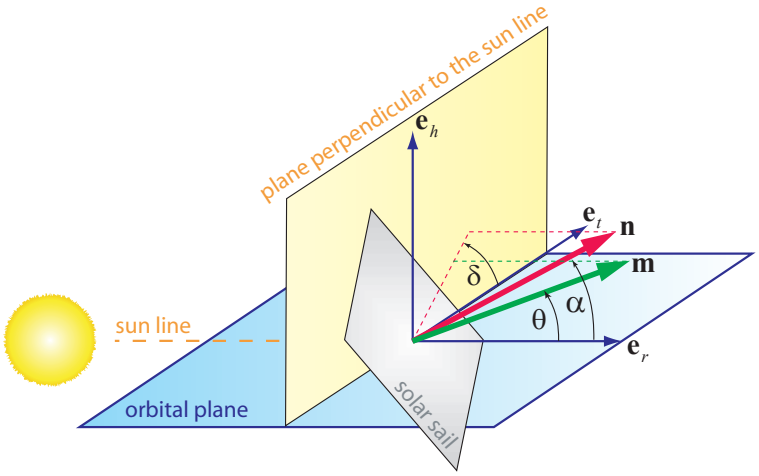

Figure 2. Definition of the sail normal vector and the trust normal vector

At a distance r from the sun, the SRP is

$$P = \frac{S_0}{c}\left(\frac{r_0}{r}\right)^2 = 4.563\,\frac{\mu\mathrm{N}}{\mathrm{m}^2}\cdot\left(\frac{r_0}{r}\right)^2 \tag{1}$$

where $S_0 = 1368\,\mathrm{W/m^2}$ is the solar constant, c is the speed of light in vacuum, and $r_0 = 1\,\mathrm{AU}$.

In this paper, the standard non-perfectly reflecting SRP force model[b] by Wright is employed, which uses the set of optical coefficients $\mathcal{P} = \{\rho, s, \varepsilon_\mathrm{f}, \varepsilon_\mathrm{b}, B_\mathrm{f}, B_\mathrm{b}\}$ to parameterize the optical characteristics of the sail film, where ρ is the reflection coefficient, s is the specular reflection factor, ε_f and ε_b are the emission coefficients of the front and back side, respectively, and B_f and B_b are the non-Lambertian coefficients of the front and back side, respectively, which describe the angular distribution of the emitted and the diffusely reflected photons. According to Wright, the optical coefficients for a solar sail with a highly reflective aluminum-coated front side and with a highly emissive chromium-coated back side (to keep the sail temperature at a moderate limit) are $\mathcal{P}_{\mathrm{Al|Cr}} = \{\rho = 0.88, s = 0.94, \varepsilon_\mathrm{f} = 0.05, \varepsilon_\mathrm{b} = 0.55, B_\mathrm{f} = 0.79, B_\mathrm{b} = 0.55\}$.[10] It can be shown[c] that in a sail-fixed 2D[d] coordinate frame $\mathcal{S} = \{\boldsymbol{n}, \boldsymbol{t}\}$ (see Fig. 3), the SRP force

[a] $\mathcal{O} = \{\boldsymbol{e}_r, \boldsymbol{e}_t, \boldsymbol{e}_h\}$ is an orthogonal right-handed polar coordinate frame. $\boldsymbol{e}_r$ points always along the sun-spacecraft line, $\boldsymbol{e}_h$ is the orbit plane normal (pointing along the spacecraft's orbital angular momentum vector), and $\boldsymbol{e}_t$ completes the right-handed coordinate system ($\boldsymbol{e}_r \times \boldsymbol{e}_t = \boldsymbol{e}_h$).

[b] See, e.g., Ref. 10 pp. 223-233, or Ref. 11 pp. 47-51, for a more detailed description of this model.

[c] See, e.g., Ref. 11 pp. 47-49 for derivation.

[d] Because of the symmetry, the third dimension is not relevant here.

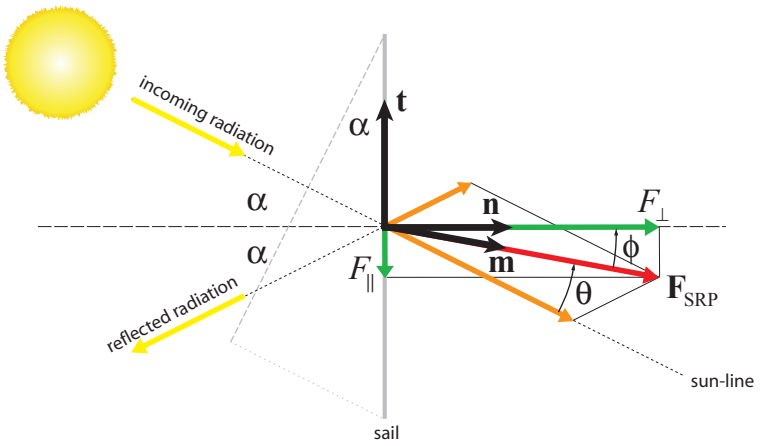

Figure 3. SRP force on a solar sail according to the non-perfectly reflecting force model

exerted on the solar sail has a normal component $F_\perp$ (along $\boldsymbol{n}$) and a tangential component $F_{||}$ (along $\boldsymbol{t}$) with

$$F_\perp = \boldsymbol{F}_{\mathrm{SRP}} \cdot \boldsymbol{n} = 2PA\cos\alpha\,\psi_\perp \tag{2a}$$
$$F_{||} = \boldsymbol{F}_{\mathrm{SRP}} \cdot \boldsymbol{t} = -2PA\cos\alpha\,\psi_{||} \tag{2b}$$

where A is the sail area and

$$\psi_\perp = a_1\cos\alpha + a_2 \tag{3a}$$
$$\psi_{||} = a_3\sin\alpha \tag{3b}$$

with

$$a_1 \triangleq \frac{1}{2}(1+s\rho) \qquad a_2 \triangleq \frac{1}{2}\left[B_\mathrm{f}(1-s)\rho + (1-\rho)\frac{\varepsilon_\mathrm{f}B_\mathrm{f} - \varepsilon_\mathrm{b}B_\mathrm{b}}{\varepsilon_\mathrm{f}+\varepsilon_\mathrm{b}}\right] \qquad a_3 \triangleq \frac{1}{2}(1-s\rho) \tag{4}$$

By defining $\Psi \triangleq (\psi_\perp^2 + \psi_{||}^2)^{1/2}$, the total SRP force vector may then be written as

$$\boldsymbol{F}_{\mathrm{SRP}} = 2PA\cos\alpha\,\Psi\,\boldsymbol{m} \tag{5}$$

where Ψ depends only on the pitch angle α and the optical coefficients $\mathcal{P}$ of the sail film. The angle between $\boldsymbol{m}$ and $\boldsymbol{n}$, $\phi = \arctan(\psi_{||}/\psi_\perp)$, is called the centerline angle. The cone angle, i.e. the angle between $\boldsymbol{m}$ and the radial unit vector $\boldsymbol{e}_r$, is then $\theta = \alpha - \phi = \alpha - \arctan(\psi_{||}/\psi_\perp)$.

The most commonly used solar sail performance parameter is the characteristic acceleration a_c. It is defined as the SRP acceleration acting on a solar sail that is oriented perpendicular to the sun line ($\boldsymbol{n} \equiv \boldsymbol{e}_r$) at r_0 (1 AU). For the non-perfectly reflecting SRP force model, it is

$$a_c = \frac{2P_0A}{m}(a_1 + a_2) \tag{6}$$

where $P_0 = P(r = r_0)$ and m is the sailcraft mass.

IV. Simulation Model

Besides the gravitational forces of all celestial bodies and the SRP force, many disturbing forces influence the motion of solar sails in space, as they are caused, e.g., by the solar wind, the finiteness of the solar disk, the reflected light from close celestial bodies, and the aberration of solar radiation (Poynting-Robertson effect). Furthermore, a real solar sail bends and wrinkles, depending on the actual solar sail design. Finally, for a mission that is to target the center of mass of a 200 m-object with a relative velocity of more than 80 km/s, relativistic corrections may have to be applied for the final targeting phase. All these issues have to be considered for high precision trajectory determination and control, as it is required for this mission.

For mission feasibility analysis, however, as it is done within this paper, the following simplifications can be made:

1. The solar sail is a flat plate.
2. The solar sail is moving under the sole influence of solar gravitation and radiation.
3. The sun is a point mass and a point light source.
4. The solar sail attitude can be changed instantaneously.

Let the reference frame $\mathcal{I} = \{\boldsymbol{e}_x, \boldsymbol{e}_y, \boldsymbol{e}_z\}$ be a heliocentric inertial right-handed cartesian coordinate frame. The equations of motion for a solar sail in the $\mathcal{I}$-frame are:

$$\dot{\boldsymbol{r}} = \boldsymbol{v}, \qquad \dot{\boldsymbol{v}} = -\frac{\mu}{r^3}\,\boldsymbol{r} + \frac{\boldsymbol{F}_{\text{SRP}}}{m} + \boldsymbol{a}_d \tag{7}$$

where $\boldsymbol{r} = (r_x, r_y, r_z)$ is the solar sail position, $\boldsymbol{v} = (v_x, v_y, v_z)$ is the solar sail velocity, μ is the sun's gravitational parameter, and $\boldsymbol{a}_d$ is the disturbing acceleration, which is – according to the simplifications made above – neglected within this paper.

V. Local and Global Trajectory Optimization Methods

A. Local Steering Laws

Local steering laws (LSLs) give the locally optimal thrust direction to change some specific osculating orbital element of the spacecraft with a locally maximum rate. To obtain LSLs, Lagrange's planetary equations in Gauss' form may be used, which describe the rate of change of a body's osculating orbital elements due to some (propulsive and/or disturbing) acceleration. This can best be done in the orbit frame $\mathcal{O} = \{\boldsymbol{e}_r, \boldsymbol{e}_t, \boldsymbol{e}_h\}$. According to Ref. 12 the equations for the semi-major axis a and the inclination i can be written as

$$\frac{da}{dt} = \frac{2a^2}{h}\left(e \sin f a_r + \frac{p}{r} a_t\right) \tag{8a}$$

$$\frac{di}{dt} = \frac{r\cos(\omega + f)}{h} a_h \tag{8b}$$

where a_r, a_t, and a_h are the acceleration components along the $\mathcal{O}$-frame unit vectors, $h = |\boldsymbol{h}|$ is the orbital angular momentum per spacecraft unit mass, and p is the semilatus rectum of the orbit. Because Eqs. (8a) and (8b) can be written as

$$\frac{da}{dt} = \begin{pmatrix} \frac{2a^2}{h} e \sin f \\ \frac{2a^2}{h}\frac{p}{r} \\ 0 \end{pmatrix} \cdot \begin{pmatrix} a_r \\ a_t \\ a_h \end{pmatrix} = \boldsymbol{k}_a \cdot \boldsymbol{a} \tag{9a}$$

$$\frac{di}{dt} = \begin{pmatrix} 0 \\ 0 \\ \frac{r\cos(\omega+f)}{h} \end{pmatrix} \cdot \begin{pmatrix} a_r \\ a_t \\ a_h \end{pmatrix} = \boldsymbol{k}_i \cdot \boldsymbol{a} \tag{9b}$$

it is clear that to decrease the semi-major axis with a maximum rate, the thrust vector has to be along the direction $-\boldsymbol{k}_a$ (local steering law $\mathcal{L}_{a^-}$). To increase the inclination with a maximum rate, the thrust vector has to be along the direction $\boldsymbol{k}_i$ ($\mathcal{L}_{i^+}$).

B. Evolutionary Neurocontrol: A Global Trajectory Optimization Method

Within this paper, evolutionary neurocontrol (ENC) is used to calculate near-globally optimal trajectories. This method is based on a combination of artificial neural networks (ANNs) with evolutionary algorithms (EAs). ENC attacks low-thrust trajectory optimization problems from the perspective of artificial intelligence and machine learning. Here, it can only be sketched how this method is used to search optimal solar sail trajectories. The reader who is interested in the details of the method is referred to Refs. 13, 14, or 15.

The problem of searching an optimal solar sail trajectory $\boldsymbol{x}^\star[t] = (\boldsymbol{r}^\star[t], \dot{\boldsymbol{r}}^\star[t])$[e] is equivalent to the problem of searching an optimal sail normal vector history $\boldsymbol{n}^\star[t]$, as it is defined by the optimal time history of the so-called direction unit vector $\boldsymbol{d}^\star[t]$, which points along the optimal thrust direction. Within the context of machine learning, a trajectory is regarded as the result of a sail steering strategy S that maps the problem relevant variables (the solar sail state $\boldsymbol{x}$ and the target state $\boldsymbol{x}_\mathrm{T}$) onto the direction unit vector, $\mathsf{S} : \{\boldsymbol{x}, \boldsymbol{x}_\mathrm{T}\} \subset \mathbb{R}^{12} \mapsto \{\boldsymbol{d}\} \subset \mathbb{R}^3$, from which $\boldsymbol{n}$ is calculated. This way, the problem of searching $\boldsymbol{x}^\star[t]$ is equivalent to the problem of searching (or learning) the optimal sail steering strategy $\mathsf{S}^\star$. An ANN may be used as a so-called neurocontroller (NC) to implement solar sail steering strategies. It can be regarded as a parameterized function $\mathsf{N}_{\boldsymbol{\pi}}$ (the network function) that is – for a fixed network topology – completely defined by the internal parameter set $\boldsymbol{\pi}$ of the ANN. Therefore, each $\boldsymbol{\pi}$ defines a sail steering strategy $\mathsf{S}_{\boldsymbol{\pi}}$. The problem of searching $\boldsymbol{x}^\star[t]$ is therefore equivalent to the problem of searching the optimal NC parameter set $\boldsymbol{\pi}^\star$. EAs that work on a population of strings can be used for finding $\boldsymbol{\pi}^\star$ because $\boldsymbol{\pi}$ can be mapped onto a string $\boldsymbol{\xi}$ (also called chromosome or individual). The trajectory optimization problem is solved when the optimal chromosome $\boldsymbol{\xi}^\star$ is found. Fig. 4 sketches the subsequent transformation of a chromosome into a solar sail trajectory. An evolutionary neurocontroller (ENC) is a NC that employs an EA for learning (or breeding) $\boldsymbol{\pi}^\star$. ENC was implemented within a low-thrust trajectory optimization program called InTrance, which stands for **In**telligent **Tra**jectory optimization using **n**euro**c**ontroller **e**volution. InTrance is a smart global trajectory optimization method that requires only the target body/state and intervals for the initial conditions (e.g., launch date, hyperbolic excess velocity, etc.) as input to find a near-globally optimal trajectory for the specified problem. It works without an initial guess and does not require the attendance of a trajectory optimization expert.

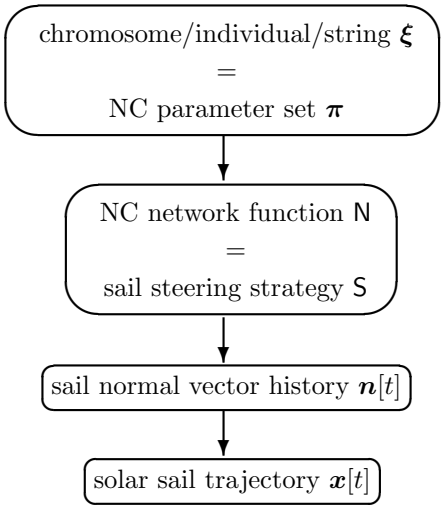

Figure 4. Transformation of a chromosome into a solar sail trajectory

VI. Results

A. Optimization of the Baseline Mission Scenario

1. Overall Description

The baseline mission scenario foresees a non-perfectly reflecting solar sail with a characteristic acceleration of $a_c = 0.5\,\mathrm{mm/s^2}$, a sail temperature limit of $T_\mathrm{lim} = 240°\mathrm{C}$, and interplanetary insertion at Earth with zero hyperbolic excess energy, $C_3 = 0\,\mathrm{km^2/s^2}$. Generally, orbits with $i < 90\,\mathrm{deg}$ are termed prograde orbits and orbits with $i > 90\,\mathrm{deg}$ are termed retrograde orbits. It was first found by Wright[16,17] and further examined by Sauer[18] that the best way to attain a retrograde orbit with a solar sail is to first spiral inwards to a solar

[e]The symbol "$[t]$" denotes the time history of the preceding variable and the symbol "$\star$" denotes its optimal value.

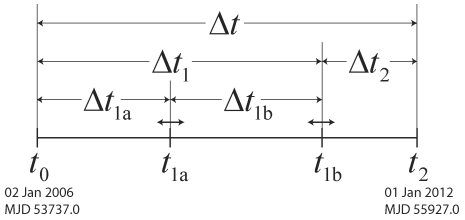

Figure 5. Mission timeline

distance that is given by the temperature limits T_{lim} of the solar sail and the spacecraft[f], and then to use the large available SRP to crank the orbit. During the orbit cranking phase, the local steering law $\mathcal{L}_{i^+}$ is applied until the desired inclination is reached. To simplify the terminology within this paper, we speak of a retrograde orbit, when the orbital angular momentum vector of the spacecraft $\boldsymbol{h}$ and the target $\boldsymbol{h}_{\mathrm{T}}$ are anti-parallel, i.e. $\angle(\boldsymbol{h}, -\boldsymbol{h}_{\mathrm{T}}) = 0\,\mathrm{deg}$. Using local steering laws, the strategy to attain such a retrograde orbit divides the trajectory into two well-defined phases

1a: Spiralling inwards until the optimum solar distance for cranking the orbit is reached using local steering law $\mathcal{L}_{a^-}$ (the inclination stays constant during phase 1a)

1b: Cranking the orbit until the orbit is retrograde using local steering law $\mathcal{L}_{i^+}$[g] (the semi-major axis stays constant during phase 1b)

Phase 1a and 1b can be regarded as a single phase, phase 1 (later, using InTrance, phase 1 will be optimized in one go). Phase 1 has to be followed by a phase 2, for which no simple LSL exists. The goal of phase 2 is to impact the target head-on with maximum relative velocity. The time that is spent for the different phases is then $\Delta t = \Delta t_1 + \Delta t_2$ with $\Delta t_1 = \Delta t_{1\mathrm{a}} + \Delta t_{1\mathrm{b}}$ ($\Delta t_{1\mathrm{a}} = t_{1\mathrm{a}} - t_0$, $\Delta t_{1\mathrm{b}} = t_{1\mathrm{b}} - t_{1\mathrm{a}}$, and $\Delta t_2 = t_2 - t_{1\mathrm{b}}$) with the constraint that the launch date is assumed fixed within this paper (see Fig. 5). As we will see later from the InTrance-solutions, using local steering laws and patching the solutions of phase 1a, 1b, and 2 together yields a suboptimal solution because a globally optimal trajectory has a smooth transition between the three phases, changing the inclination also slightly during phase 1a and 2, whenever the sailcraft is close to the nodes. Therefore, we define $t_{1\mathrm{b}}$, the end of phase 1, as follows: let $\Delta i_{\measuredangle_{\mathrm{T}}} = |i_{\measuredangle_{\mathrm{T}}} - i|$ be the difference between the inclination i of the spacecraft and the inclination of the retrograde target orbit, $i_{\measuredangle_{\mathrm{T}}} = |180\,\mathrm{deg} - i_{\mathrm{T}}|$. Then $t = t_{1\mathrm{b}}$, when $\Delta i_{\measuredangle_{\mathrm{T}}} = 10\,\mathrm{deg}$. This means that at the end of phase 1 the sailcraft orbit does not have to be *exactly* retrograde because this can be accounted for within phase 2.

2. Determination of the Optimal Orbit Cranking Radius

If solar sail degradation is not considered, the acceleration capability of the solar sail increases $\propto 1/r^2$ when going closer to the sun. The minimum solar distance, however, is constrained by the temperature limit of the sail film T_{lim} and the spacecraft. Here, however, only the temperature limit of the sail film is considered. The equilibrium temperature of the sail film is[h]

$$T = \left[\frac{S_0}{\sigma}\frac{1-\rho}{\varepsilon_{\mathrm{f}}+\varepsilon_{\mathrm{b}}}\left(\frac{r_0}{r}\right)^2\cos\alpha\right]^{1/4} \tag{10}$$

where $\sigma = 5.67\times10^{-8}\,\mathrm{Wm^{-2}K^{-4}}$ is the Stefan-Boltzmann constant. Thus, the sail temperature does not only depend on the solar distance, but also on the sail attitude, $T = T(r,\alpha)$ (and of course on the set of optical parameters $\mathcal{P}$ that is assumed as fixed within this paper). It was demonstrated in Ref. 19 that faster trajectories can be obtained for a given sail temperature limit T_{lim}, if not a minimum solar distance r_{lim} but T_{lim} is used directly as a constraint. This can be realized by constraining the pitch angle α (that is also the light incidence angle) in a way that it cannot become smaller than the critical pitch angle, where T_{lim} would be exceeded, i.e. $\alpha > \alpha_{\mathrm{lim}}(r, T_{\mathrm{lim}})$.

[f]However, although the sail temperature depends not only on the solar distance but also on the pitch angle, as it will be seen later, Sauer used a minimal solar distance r_{lim} instead of a temperature limit T_{lim}.

[g]Thereby, it might be necessary to change the ascending node of the orbit, so that the inclination change is $\leq 180\,\mathrm{deg}$.

[h]See, e.g., Ref. 11 pp. 48-49 for derivation.

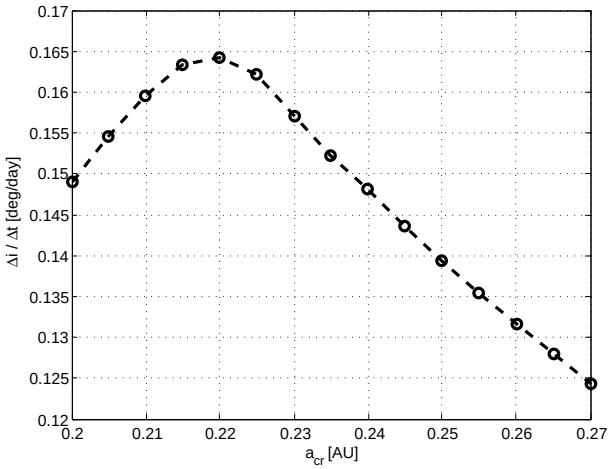

Figure 6. Baseline Mission Scenario: Dependence of inclination change rate on orbit cranking radius (circular orbit)

Although orbit cranking is most effective for a circular orbit, it is also important to consider elliptic orbits. Therefore, we describe the optimal orbit cranking behavior rather by an orbit cranking semi-major axis $a_{\rm cr}$ instead of an orbit cranking radius. Using the direct sail temperature constraint, $a_{\rm cr}$ defines the time $\Delta t_{1\rm b}$ that is required to make the orbit retrograde. $\Delta t_{1\rm b}$ is influenced by two adverse effects, leading to an optimal orbit cranking semi-major axis $a_{\rm cr,opt}(T_{\rm lim})$ where the inclination change rate $\Delta i/\Delta t$ is maximal an thus $\Delta t_{1\rm b}$ is minimal, as it can be seen from Fig. 6. For $a_{\rm cr} > a_{\rm cr,opt}$, the inclination change takes longer than for $a_{\rm cr,opt}$ because of the lower SRP. For $a_{\rm cr} < a_{\rm cr,opt}$, the inclination change also takes longer than for $a_{\rm cr,opt}$ because of the (inefficiently) large critical pitch angle $\alpha_{\rm lim}$ that is required to keep $T < T_{\rm lim}$. Thus $\Delta t_{1\rm b} = \Delta t_{1\rm b}(T_{\rm lim})$. It can seen from Fig. 6 that $a_{\rm cr,opt}(T_{\rm lim} = 240^\circ{\rm C}) = 0.22\,{\rm AU}$ where $\Delta i/\Delta t = 0.1642\,{\rm deg/day}$.

3. Calculation of Phase 1 Using Local Steering Laws

Knowing now that the optimal semi-major axis for orbit cranking is 0.22 AU, we can calculate an estimate for Δt_1 using the local steering laws $\mathcal{L}_{a^-}$ (phase 1a, $\Rightarrow \Delta t_{1\rm a}$) and $\mathcal{L}_{i^+}$ (phase 1b, $\Rightarrow \Delta t_{1\rm b}$). The trajectories for both phases are shown in Figs. 7(a) and 7(b). Fig. 7(c) shows a very sharp transition between phase 1a and 1b. The time that is required for spiralling to $a_{\rm cr,opt}$ is $\Delta t_{1\rm a} = 635.5\,{\rm days}$. If the final spacecraft state of phase 1a is taken as the initial spacecraft state for phase 1b, the time that is required for cranking the orbit to $\Delta i_{\curvearrowright_{\rm T}} = 10\,{\rm deg}$ is $\Delta t_{1\rm b} = 973.5\,{\rm days}$. Therefore, the duration of phase 1 is $\Delta t_1 = 1609\,{\rm days}$. Note that this calculation did not include the alignment of the ascending node of the sailcraft Ω with the ascending node of the retrograde asteroid orbit $\Omega_{\curvearrowright_{\rm T}}$, so that $\Delta\Omega_{\curvearrowright_{\rm T}}(t_{1\rm b}) = |\Omega_{\curvearrowright_{\rm T}}(t_{1\rm b}) - \Omega(t_{1\rm b})| = 56.7\,{\rm deg}$. This misalignment, however, could be removed by optimizing the launch date t_0. Note that, when $\mathcal{L}_{a^-}$ is applied, the trajectory has generally some eccentricity at $a = a_{\rm cr,opt}$. If we do not use the final spacecraft state of phase 1a as the initial state for phase 1b, but assume a circular orbit to get the lower bound for what can be achieved with local steering laws, we get $\Delta t_{1\rm b} = 960\,{\rm days}$ for $\Delta i_{\curvearrowright_{\rm T}} = 10\,{\rm deg}$, which is only 13.5 days less ($\Delta t_1 = 1595.5\,{\rm days}$).

4. Optimization of Phase 1 Using InTrance

Using InTrance, phase 1 is optimized in one go. InTrance yields $\Delta t_1 = 1572\,{\rm days}$, which is 37 days (2.4%) faster than the LSL solution. Fig. 8(c) now shows a very smooth transition between phase 1a and 1b. This result proves that a global optimal solution changes the inclination also during phase 1a, whenever the solar sail is close to the nodes. Due to the poor *local* search behavior of InTrance, few "spikes" remain in the control angles (Fig. 8(d)), so that further fine-tuning of the solution might yield a marginally shorter trajectory. The orientation of the final orbit is well aligned with the retrograde asteroid orbit, $\Delta\Omega_{\curvearrowright_{\rm T}}(t_{1\rm b}) = 1.3\,{\rm deg}$.

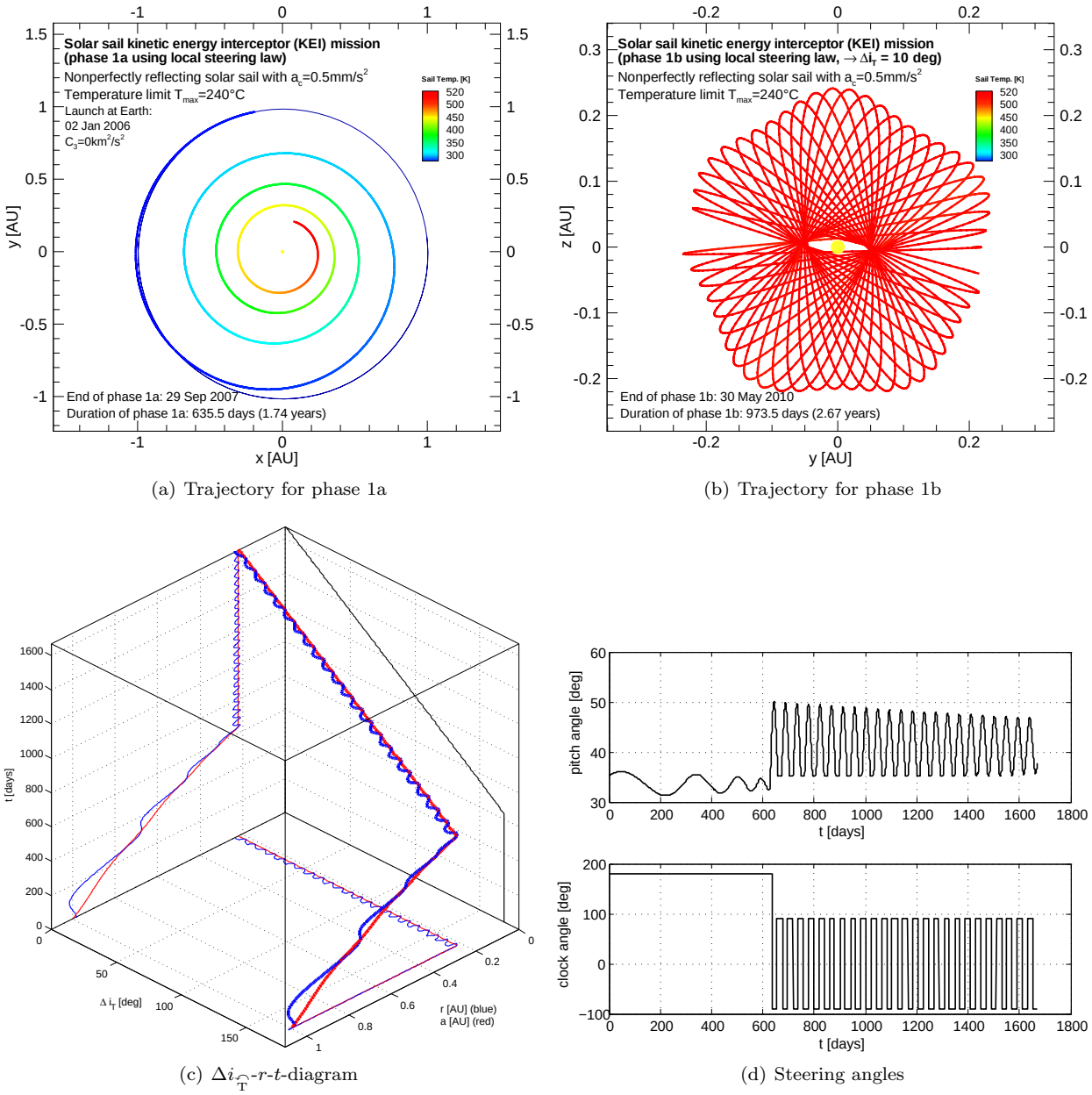

(a) Trajectory for phase 1a

(b) Trajectory for phase 1b

(c) $\Delta i_{\widehat{T}}$-r-t-diagram

(d) Steering angles

Figure 7. Baseline Mission Scenario: phase 1, local steering law solution

5. Optimization of Phase 1 Using a Combination of InTrance and $\mathcal{L}_{i^+}$ (InTrance & $\mathcal{L}_{i^+}$)

Looking at Fig. 8(c), one sees that a_{cr} is not constant during phase 1b. Additional to the "spikes" in the control angles (Fig. 8(d)), this indicates also that the InTrance solution is not locally optimal. Therefore, we have applied a combination of InTrance with the local steering law $\mathcal{L}_{i^+}$, using InTrance until $a = a_{\mathrm{cr,opt}}$ and $\mathcal{L}_{i^+}$ from this point on. The results are shown in Fig. 9. This strategy yields $\Delta t_1 = 1564\,\mathrm{days}$, showing that the InTrance-solution for phase 1b was suboptimal, however, only very slightly (8 days, 0.5%). This result proves that the InTrance-solution is close to the global optimum, but local fine-tuning can slightly improve the solution. The orientation of the final orbit is well aligned with the retrograde asteroid orbit, $\Delta\Omega_{\widehat{T}}(t_{1\mathrm{b}}) = 1.5\,\mathrm{deg}$.

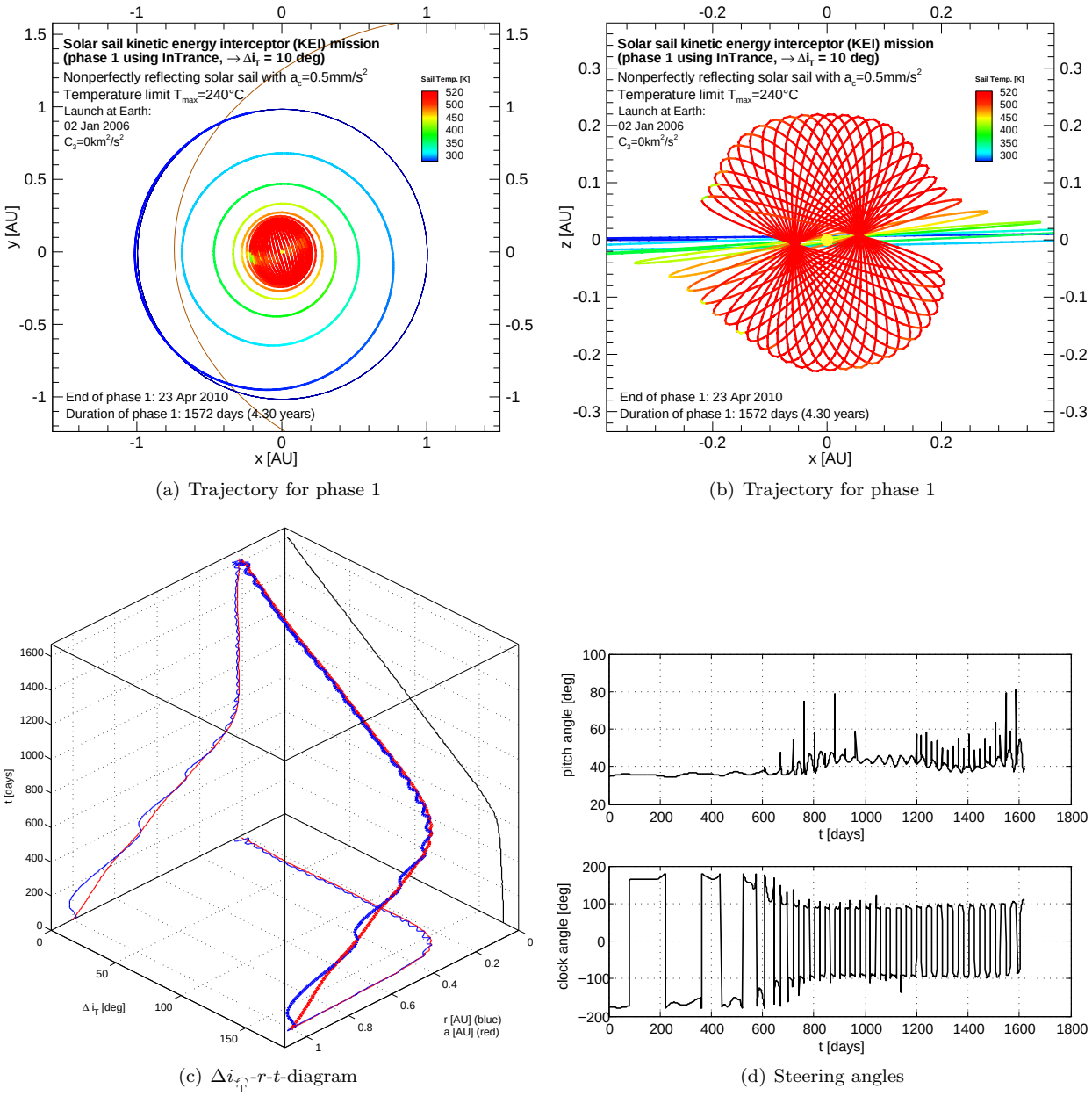

(a) Trajectory for phase 1

(b) Trajectory for phase 1

(c) $\Delta i_{\widehat{T}}$-r-t-diagram

(d) Steering angles

Figure 8. Baseline Mission Scenario: phase 1, InTrance-solution

6. *Optimization of Phase 2*

The simplest approach to deflect a NEA is to impact it with a massive projectile at a high relative velocity. A successful asteroid deflection mission, however, will require accurate modeling and prediction of the velocity change caused by the impactor. The effective impulse imparted to the asteroid will be the sum of the pure kinetic impulse (linear momentum) of the impactor plus the impulse due to the "thrust" of material being ejected from the impact crater. The last term can be very significant (even dominant), but its magnitude depends strongly upon the density and yield strength of the material of which the asteroid is composed, as well as the mass and relative velocity of the impactor. For example, a head-on collision (at a relative velocity of $v_{\mathrm{imp}} = 80\,\mathrm{km/s}$) of a 150 kg impactor on a 200 m S-class asteroid (with a density of $2\,720\,\mathrm{kg/m^3}$) yields a pure kinetic-impact Δv of approx. 0.1 cm/s. If the asteroid is composed of hard rock, then the modeling of crater ejecta impulse from previous studies would predict an additional Δv of 0.2 cm/s, which is double

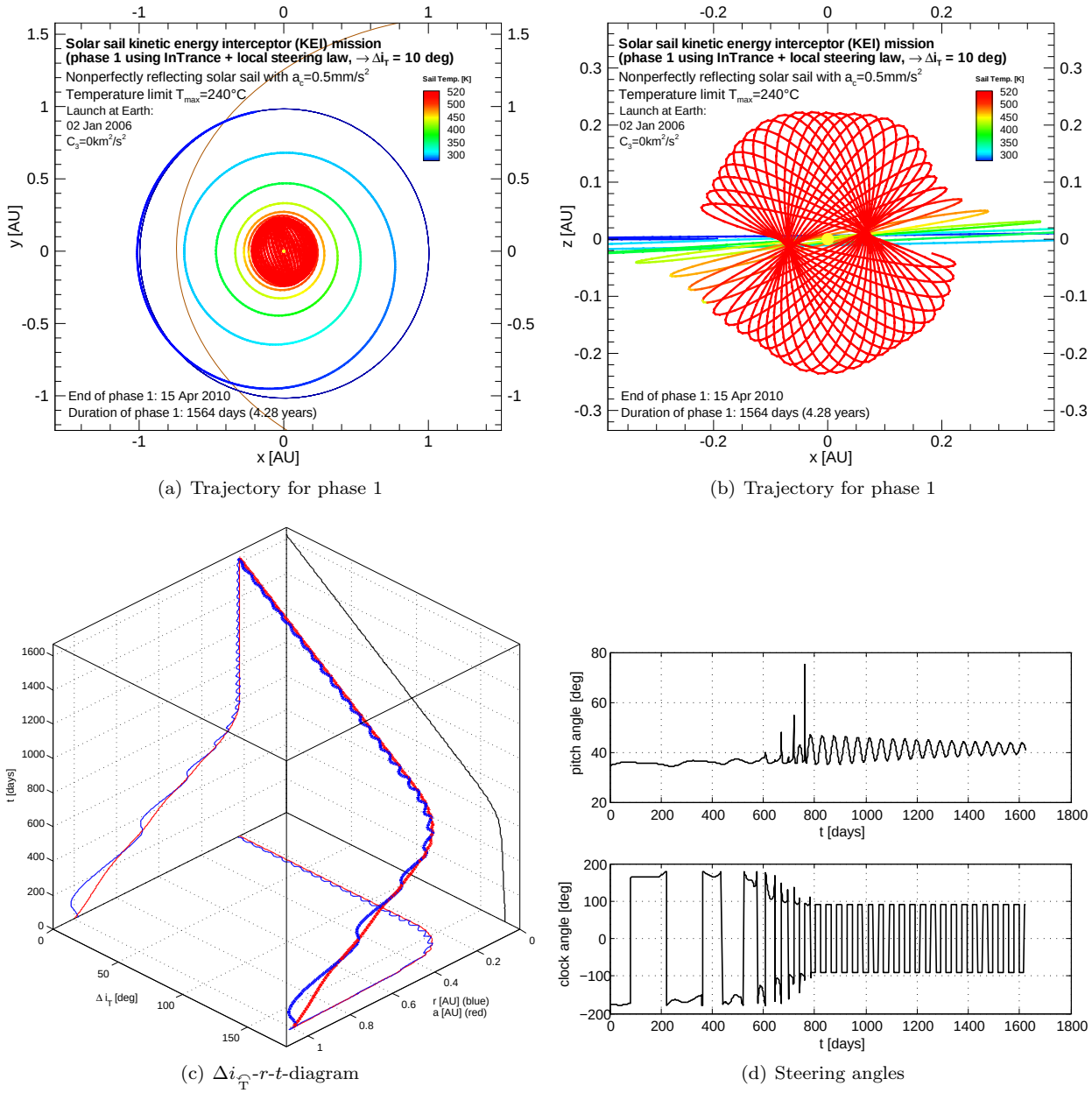

(a) Trajectory for phase 1

(b) Trajectory for phase 1

(c) $\Delta i_{\widehat{T}}$-r-t-diagram

(d) Steering angles

Figure 9. Baseline Mission Scenario: phase 1, combination of InTrance-solution and local steering law

the pure kinetic-impact Δv.[20,21] If the asteroid were composed of soft rock, however, the previous studies would instead predict an additional Δv of 0.6 cm/s, which is about six times the pure kinetic-impact Δv. An accurate modeling and prediction of the ejecta impulse for various asteroid compositions is therefore a critical part of kinetic-impact approaches. A practical concern of any kinetic-impact approach is the risk that the impact could result in the fragmentation of the asteroid, which could substantially increase the damage upon Earth impact.[22] The energy required to fragment an asteroid depends critically upon its composition and structure. For example, for a 200 m asteroid composed largely of ice, the disruption energy is approximately 3.4×10^{10} J. Because the kinetic energy of a 150 kg impactor at a relative velocity of 80 km/s would be 4.8×10^{11} J, the ice asteroid would likely fragment.[23] If the asteroid was composed largely of silicates, it would have a disruption energy of approximately 2.3×10^{12} J, about five times larger than the kinetic energy delivered by the impactor; this asteroid would likely stay intact.[23] Therefore, further studies are needed to optimize impactor size, relative impact velocity, and the total number of impactors as functions of the

asteroid's size and composition, to ensure that the impact does not cause fragmentation.

For the following calculations, it is assumed that a head-on collision with a relative velocity $v_{\mathrm{imp}} = 70\,\mathrm{km/s}$ at the asteroids perihelion leads to a change of the asteroids orbital velocity of $\Delta v_{\mathrm{NEA,imp}} = 0.3\,\mathrm{cm/s}$ (see Ref. 23). Thus, assuming that $\Delta v_{\mathrm{NEA,imp}}$ varies proportional to v_{imp}, we can assume for simplicity (without further impact modeling) a collision efficiency factor of $\frac{\Delta v_{\mathrm{NEA,imp}}}{v_{\mathrm{imp}}} = 4.3 \times 10^{-8}$. Therefore, the goal of phase 2 is to maximize the head-on impact velocity. The optimization objective used for InTrance was: maximize $\boldsymbol{v} \cdot (-\boldsymbol{v}_{\mathrm{NEA}})$! Fig. 10 shows the resulting trajectory and the orbital elements that define the shape and inclination of the orbit.

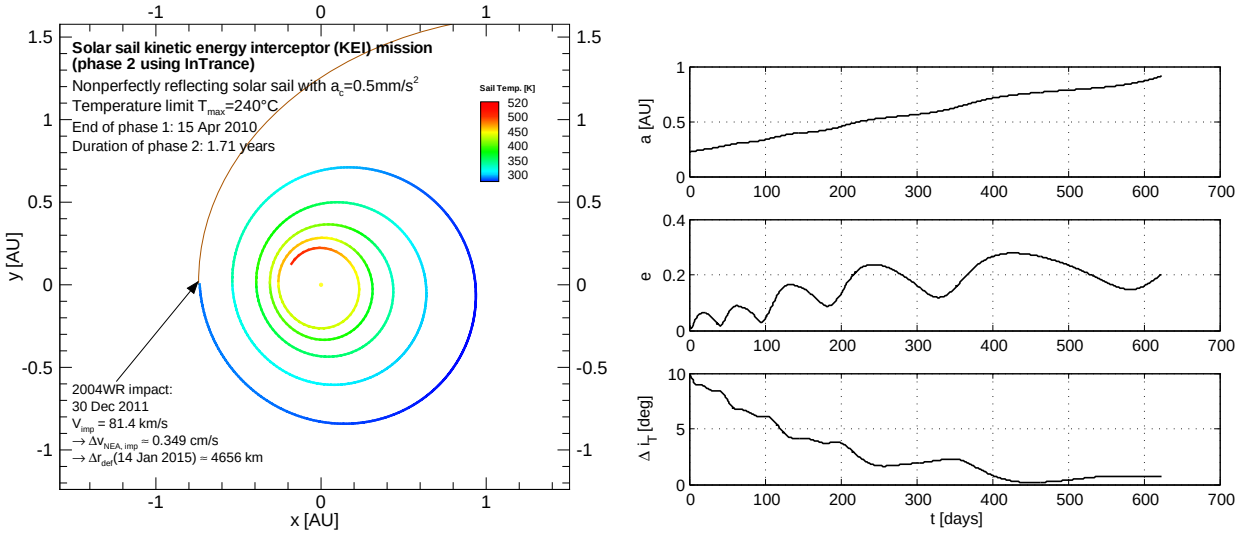

(a) Trajectory for phase 2

(b) Selected orbital elements

Figure 10. Baseline Mission Scenario: phase 2, InTrance-solution

InTrance achieves an impact velocity of 81.4 km/s. This yields $\Delta v_{\mathrm{NEA,imp}} = 0.349\,\mathrm{cm/s}$. Numerical integration of the asteroids orbit after the impact, including all planetary disturbances, yields a deflection distance of $\Delta r_{\mathrm{defl}} = 4656\,\mathrm{km}$ (0.73 Earth radii) at 14 Jan 2015, the date of Earth impact. It is clear that the impact velocity depends only on the characteristic acceleration of the sailcraft and the time Δt_2 that is available after phase 1 to maximize the impact velocity, thus $v_{\mathrm{imp}} = v_{\mathrm{imp}}(a_c, \Delta t_2)$. Having evaluated several post-impact calculations, the deflection distance (for this scenario!) can be approximated with an error of less than 0.1% (with the assumptions of the impact model) by

$$\widetilde{\Delta r}_{\mathrm{defl}} \approx 57.16 \cdot \tilde{v}_{\mathrm{imp}} \tag{11}$$

where the tilde denotes dimensionless variables, $\widetilde{\Delta r}_{\mathrm{defl}} = \frac{\Delta r_{\mathrm{defl}}}{1\,\mathrm{km}}$ and $\tilde{v}_{\mathrm{imp}} = \frac{v_{\mathrm{imp}}}{1\,\mathrm{km/s}}$.

B. Variation of the Hyperbolic Excess Energy for Interplanetary Insertion

In this section, the influence of the hyperbolic excess energy[i] C_3 on the mission performance is investigated. To find out how C_3 influences the time that is available for phase 2 to gain orbital energy, we have used InTrance to calculate $\Delta t_1(C_3)$. This gives then $\Delta t_2(C_3) = \Delta t - \Delta t_1(C_3)$. The results are shown in Fig. 11(a). As expected, the time that is available for phase 2 increases with C_3. For $0\,\mathrm{km^2/s^2} \le C_3 \le 100\,\mathrm{km^2/s^2}$, it can be approximated with an error of less than 10% by

$$\widetilde{\Delta t}_2 = 626 + 68.5 \cdot \tilde{C}_3^{0.4} \tag{12}$$

where $\widetilde{\Delta t}_2 = \frac{\Delta t_2}{1\,\mathrm{day}}$ and $\tilde{C}_3 = \frac{C_3}{1\,\mathrm{km^2/s^2}}$. We have also investigated how the time that is available for phase 2 influences the impact velocity. For this purpose, we have taken the spacecraft state of the reference trajectory at $t_{1\mathrm{b}}$ as initial state for phase 2, but set the date back by 50, 100, 150, and 200 days, so that this time is

[i] C_3 depends mainly on the size of the launch vehicle.

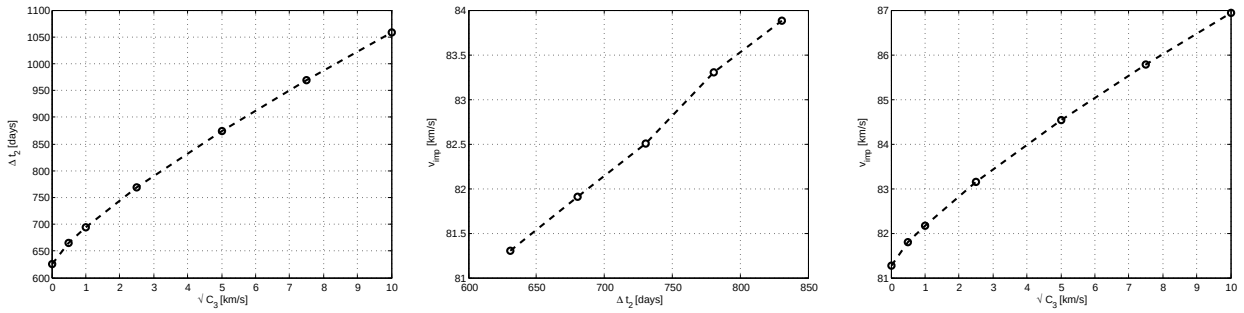

(a) Δt_2 over C_3 (b) v_{imp} over Δt_2 (c) v_{imp} over C_3

Figure 11. Variation of C_3 ($a_c = 0.5\,\mathrm{mm/s^2}$, $T_{\mathrm{lim}} = 240^\circ\mathrm{C}$)

additionally available for the sail to gain orbital energy for the impact. The results are shown in Fig. 11(b). As expected, the impact velocity increases with the duration of phase 2. For $600\,\mathrm{days} \lesssim \Delta t_2 \lesssim 850\,\mathrm{days}$, it can be approximated with an error of less than 0.1% by

$$\tilde{v}_{\mathrm{imp}} \approx 73.017 + 0.0131 \cdot \widetilde{\Delta t}_2 \tag{13}$$

Combining Eqs. (12) and (13), we can approximate the impact velocity for $0\,\mathrm{km^2/s^2} \lesssim C_3 \lesssim 25\,\mathrm{km^2/s^2}$ by

$$\tilde{v}_{\mathrm{imp}} \approx 81.218 + 0.897 \cdot \tilde{C}_3^{0.4} \tag{14}$$

C. Variation of the Sail Temperature Limit

In this section, the influence of the solar sail temperature limit T_{lim} on the mission performance is investigated. Fig. 12 shows for a circular orbit $(\Delta i/\Delta t)(a_{\mathrm{cr}})$ for different solar sail temperature limits. For $200^\circ\mathrm{C} \leq T_{\mathrm{lim}} \leq 260^\circ\mathrm{C}$, the optimal orbit cranking semi-major axis can be approximated with an error of less than 1% by

$$\tilde{a}_{\mathrm{cr,opt}} \approx 30 \cdot \tilde{T}_{\mathrm{lim}}^{-0.897} \tag{15}$$

where $\tilde{a}_{\mathrm{cr,opt}} = \frac{a_{\mathrm{cr,opt}}}{1\,\mathrm{AU}}$ and $\tilde{T}_{\mathrm{lim}} = \frac{T_{\mathrm{lim}}}{1^\circ\mathrm{C}}$. The maximum inclination change rate can be approximated with an error of less than 1% by

$$\widetilde{(\Delta i/\Delta t)}_{\max} \approx 9.26 \times 10^{-4} \cdot \tilde{T}_{\mathrm{lim}} - 5.68 \times 10^{-2} \tag{16}$$

where $\widetilde{(\Delta i/\Delta t)}_{\max} = \frac{(\Delta i/\Delta t)_{\max}}{1\,\mathrm{deg/day}}$.

We used InTrance to optimize phase 1 for different solar sail temperature limits ($200^\circ\mathrm{C} \leq T_{\mathrm{lim}} \leq 260^\circ\mathrm{C}$). The results are shown in Table 1 and Fig. 13. Fig. 13(b) shows that InTrance matches the optimal orbit cranking semi-major axes shown in Fig. 12 very closely. For $200^\circ\mathrm{C} \leq T_{\mathrm{lim}} \leq 260^\circ\mathrm{C}$, the time required for phase 1 can be approximated with an error of less than 1% by

$$\widetilde{\Delta t}_1 \approx 8.05 \times 10^4 \cdot \tilde{T}_{\mathrm{lim}}^{-0.718} \tag{17}$$

so that the time that is available for phase 2 can be approximated by

$$\widetilde{\Delta t}_2 \approx 2190 - 8.05 \times 10^4 \cdot \tilde{T}_{\mathrm{lim}}^{-0.718} \tag{18}$$

Using then Eq. (13), the impact velocity can be approximated (with an error of less than 0.25%) by

$$\tilde{v}_{\mathrm{imp}} \approx 101.7 - 1055 \cdot \tilde{T}_{\mathrm{lim}}^{-0.718} \tag{19}$$

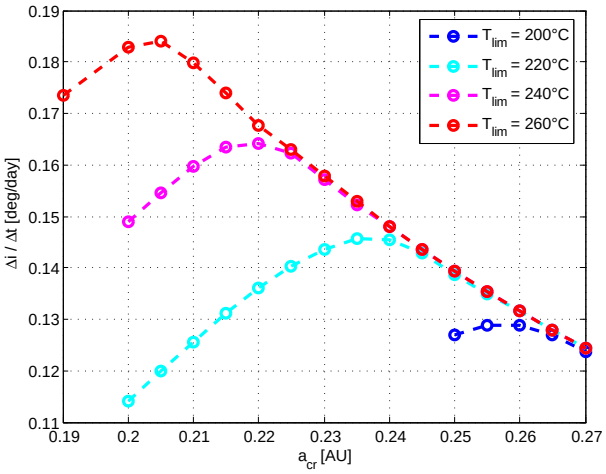

Figure 12. Dependence of the inclination change rate on orbit cranking radius for different solar sail temperature limits (circular orbit)

Table 1. Variation of $T_{\lim}$ ($a_c = 0.5\,\mathrm{mm/s^2}$, $C_3 = 0\,\mathrm{km^2/s^2}$, InTrance & $\mathcal{L}_{i+}$)

$T_{\lim}$ [°C]	$a_{\mathrm{cr,opt}}$ [AU]	$(\Delta i/\Delta t)_{\max}$ [deg/day]	Δt_1	Δt_2	$\tilde{v}_{\mathrm{imp}}$	$\widetilde{\Delta r}_{\mathrm{defl}}$
200	0.260	0.1291	1806	384	78.0	4460
220	0.236	0.1461	1661	529	79.9	4570
240	0.220	0.1648	1564	626	81.2	4640
260	0.205	0.1838	1494	696	82.1	4690

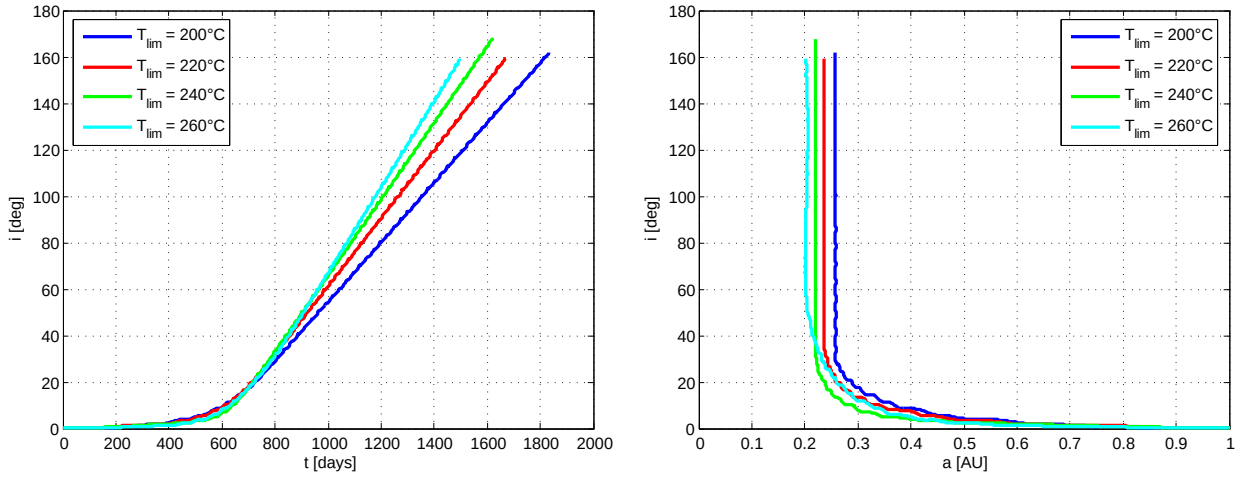

(a) inclination over flight time, $i(t)$

(b) inclination over semi-major axis, $i(a)$

Figure 13. Phase 1, optimized with InTrance: variation of $T_{\lim}$ ($a_c = 0.5\,\mathrm{mm/s^2}$, $C_3 = 0\,\mathrm{km^2/s^2}$)

D. Variation of the Characteristic Acceleration

In this section, the influence of the characteristic acceleration a_c on the mission performance is investigated. We used InTrance to optimize phase 1 for different characteristic accelerations ($0.5\,\mathrm{mm/s^2} \leq a_c \leq 0.6\,\mathrm{mm/s^2}$). The results are shown in Table 2 and Fig. 14. Fig. 14(b) shows that the optimal orbit cranking semi-major axis is independent of a_c. For $0.5\,\mathrm{mm/s^2} \leq a_c \leq 0.6\,\mathrm{mm/s^2}$, the maximum inclination change

Table 2. Variation of a_c ($T_{\lim} = 240°\mathrm{C}$, $C_3 = 0\,\mathrm{km^2/s^2}$, InTrance & $\mathcal{L}_{i+}$)

a_c [mm/s^2]	$(\Delta i/\Delta t)_{\max}$ [deg/day]	Δt_1 [days]	Δt_2 [days]	v_{imp} [km/s]	Δr_{defl} [km]
0.5	0.1642	1564	626	81.4	4656
0.55	0.1803	1425	765	83.8	4791
0.6	0.1963	1323	867	85.0	4857

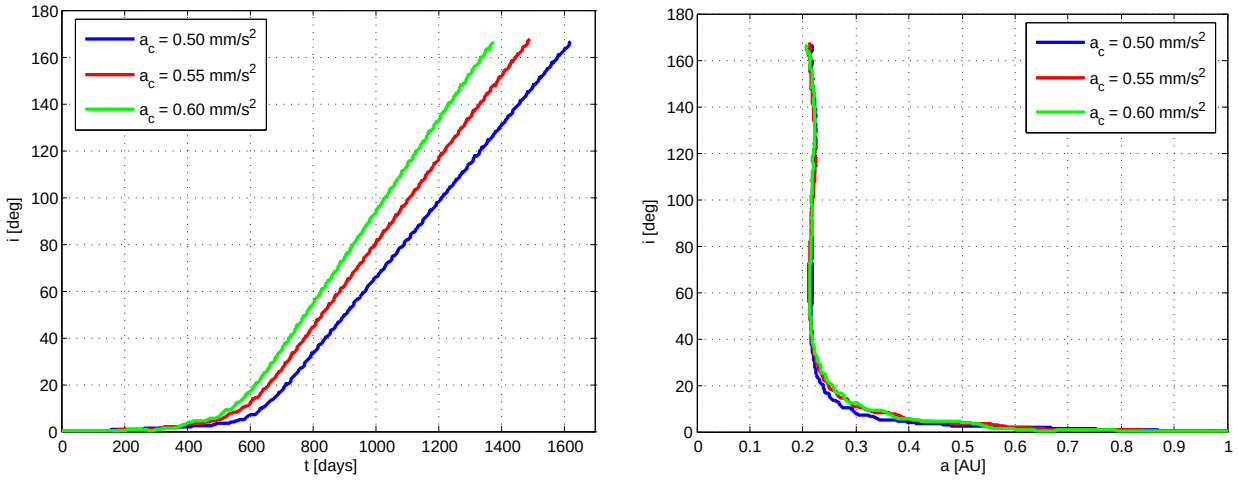

(a) inclination over flight time, $i(t)$

(b) inclination over semi-major axis, $i(a)$

Figure 14. Phase 1, optimized with InTrance: variation of a_c ($T_{\lim} = 240°\mathrm{C}$, $C_3 = 0\,\mathrm{km^2/s^2}$)

rate can be approximated with an error of less than 0.1% by

$$\widetilde{(\Delta i/\Delta t)}_{\max} \approx 0.3238 \cdot \tilde{a}_c^{0.9794} \tag{20}$$

where $\tilde{a}_c = \frac{a_c}{1\,\mathrm{mm/s^2}}$. The duration of phase 1 can then be approximated with an error of less than 0.4% by

$$\widetilde{\Delta t}_1 \approx 297.1 \cdot \tilde{a}_c^{-0.8257} + \frac{170}{0.3238 \cdot \tilde{a}_c^{0.9794}} \approx 297.1 \cdot \tilde{a}_c^{-0.8257} + 525 \cdot \tilde{a}_c^{-0.9794} \tag{21}$$

The duration of phase 2 is then approximately

$$\widetilde{\Delta t}_2 \approx 2190 - 297.1 \cdot \tilde{a}_c^{-0.8257} - 525 \cdot \tilde{a}_c^{-0.9794} \tag{22}$$

E. Solar Sail Degradation

To investigate the effects of optical degradation of the sail film, as it is expected in the extreme space environment close to the sun, we apply here the parametric model developed in Refs. 24 and 25. In this parametric model the optical parameters p are assumed to depend on the cumulated solar radiation dose (SRD) $\Sigma(t)$ on the sail:

$$\frac{p(t)}{p_0} = \begin{cases} \left(1 + d\mathrm{e}^{-\lambda\Sigma(t)}\right) / (1+d) & \text{for} \quad p \in \{\rho, s\} \\ 1 + d\left(1 - \mathrm{e}^{-\lambda\Sigma(t)}\right) & \text{for} \quad p = \varepsilon_{\mathrm{f}} \\ 1 & \text{for} \quad p \in \{\varepsilon_{\mathrm{b}}, B_{\mathrm{f}}, B_{\mathrm{b}}\} \end{cases} \tag{23}$$

The (dimensionless) SRD is

$$\Sigma(t) = \frac{\tilde{\Sigma}(t)}{\tilde{\Sigma}_0} = \left(r_0^2 \int_{t_0}^{t} \frac{\cos\alpha}{r^2}\, dt' \right) \Big/ 1\,\mathrm{yr} \tag{24}$$

with $\tilde{\Sigma}_0 \triangleq S_0 \cdot 1\,\mathrm{yr} = 1368\,\mathrm{W/m^2} \cdot 1\,\mathrm{yr} = 15.768\,\mathrm{TJ/m^2}$ being the annual SRD on a surface perpendicular to the sun at 1 AU. The degradation constant λ is related to the "half life solar radiation dose" $\hat{\Sigma}$ ($\Sigma = \hat{\Sigma} \Rightarrow p = \frac{p_0+p_\infty}{2}$) via

$$\lambda = \frac{\ln 2}{\hat{\Sigma}} \tag{25}$$

The degradation factor d defines the end-of-life values p_∞ of the optical parameters:

$$\rho_\infty = \frac{\rho_0}{1+d} \qquad s_\infty = \frac{s_0}{1+d} \qquad \varepsilon_{\mathrm{f}\infty} = (1+d)\varepsilon_{\mathrm{f}0}$$
$$\varepsilon_{\mathrm{b}\infty} = \varepsilon_{\mathrm{b}0} \qquad B_{\mathrm{f}\infty} = B_{\mathrm{f}0} \qquad B_{\mathrm{b}\infty} = B_{\mathrm{b}0}$$

Table 3 and Fig. 15 show the results for different degradation factors $0 \le d \le 0.2$, assuming a half life SRD of $25\,S_0 \cdot 1\,\mathrm{yr} = 394\,\mathrm{TJ/m^2}$. It can be seen from Table 3 that for $d > 0.05$ it is not possible to meet the mission objective. The time that is available for phase 2 is to short to make an impact with the target. Fig. 15(b) shows that for larger degradation factors it is favorable to make the orbit cranking further away from the sun than it would be optimal without degradation. The main degradation effect can be seen from Fig. 15(a), which shows that $\Delta i/\Delta t$ becomes smaller with increasing SRD. Because the underestimation of optical degradation could be a show-stopper for this mission, and because the real degradation behavior of solar sails in the space environment is to considerable degree indefinite, extensive ground and in-space tests are required prior to this mission.

Table 3. Variation of the optical degradation factor (InTrance)

d	Δt_1 [days]	Δt_2 [days]	v_{imp} [km/s]	Δr_{defl} [km]
0.0	1572	618	81.4	4640
0.05	1705	485	79.4	4540
0.1	1839	351	–	–
0.2	2074	116	–	–

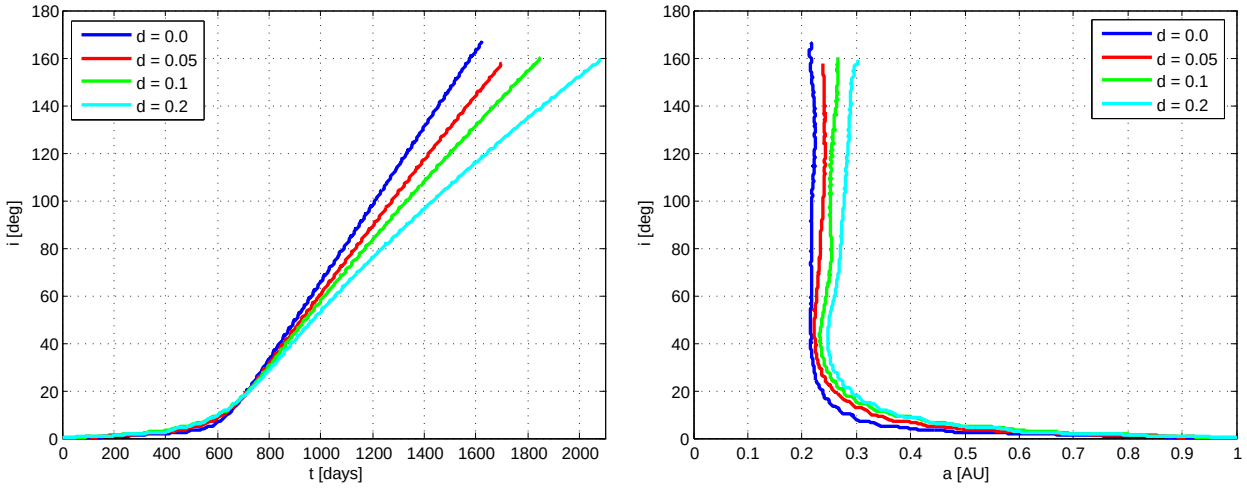

(a) inclination over flight time, $i(t)$

(b) inclination over semi-major axis, $i(a)$

Figure 15. Phase 1, optimized with InTrance: different optical degradation factors ($a_c = 0.5\,\mathrm{mm/s^2}$, $T_{\mathrm{lim}} = 240°\mathrm{C}$, $C_3 = 0\,\mathrm{km^2/s^2}$)

VII. Summary and Conclusions

We have shown that solar sails are a realistic option to deflect a fictional 200 m diameter asteroid with a kinetic impact. The required technology for such a mission, however, is not yet state-of-the-art, but would have to be developed in a sharply pursued technological program within the next 20 years. In our baseline scenario, we have used a non-perfectly reflecting solar sail with a maximum acceleration of $0.5\,\mathrm{mm/s^2}$ at 1 AU to transport a separable 150 kg impactor to the target within 6 years. A sail temperature limit of 240°C was assumed and zero hyperbolic excess energy for interplanetary insertion. We have shown that such a sailcraft is able to impact the asteroid with a relative head-on velocity of 81.4 km/s at its perihelion, leading to an estimated deflection of more than a half Earth radius. Thereby, we have found that a global trajectory optimization technique yields larger impact velocities than they can be achieved with local steering laws. The impact velocity can be increased by a considerable amount either by using a lighter solar sail, or by using a more temperature-resistant sail, or by inserting the sailcraft with a larger hyperbolic excess velocity at Earth. We have also found that the mission performance might be seriously affected by optical degradation of the sail surface, as it is expected in the extreme space environment close to the sun. However, because the real degradation behavior of solar sails in the space environment is to considerable degree indefinite, ground and in-space tests are required prior to this mission. Other problems that have to be considered for the design of this mission are the extreme requirements for the terminal guidance prior to impact (accuracy much better than 100 m at a relative velocity of more than 80 km/s) and the thermal control that has to withstand very close solar distances ($0.2 - 0.25$ AU).

Acknowledgements

The constructive comments of Malcolm Macdonald and Ian Carnelli on the manuscript are greatly appreciated.

References

[1]European Asteroid Research Node Website, http://earn.dlr.de.

[2]Commitee on Planetary and Lunar Exploration, Space Studies Board, and Commission on Physical Sciences, Mathematics, and Applications, "The Exploration of Near-Earth Objects," Tech. rep., National Research Council, 1998.

[3]Ward, P. and Brownlee, D., *Rare Earth. Why Complex Life Is Uncommon in the Universe*, Copernicus, New York, 2000.

[4]Gladman, B., Michel, P., and Froeschle, C., "The Near-Earth Object Population," *Icarus*, Vol. 146, 2000, pp. 176–189.

[5]de Pater, I. and Lissauer, J., *Planetary Sciences*, Cambridge University Press, Cambridge, New York, Melbourne, 2001.

[6]McInnes, C., "Deflection of Near-Earth Asteroids by Kinetic Energy Impacts From Retrograde Orbits," *Planetary and Space Science*, Vol. 52, 2004, pp. 587–590.

[7]Blume, W., "Deep Impact: Mission Design Approach for a New Discovery Mission," *Acta Astronautica*, Vol. 52, No. 2-6, 2003, pp. 105–110.

[8]NASA's Deep Impact Mission Web Site, http://deepimpact.jpl.nasa.gov.

[9]ESA's Don Quijote Mission Web Site, http://www.esa.int/gsp/NEO/quijote/quijote.htm.

[10]Wright, J., *Space Sailing*, Gordon and Breach Science Publishers, Philadelphia, 1992.

[11]McInnes, C., *Solar Sailing. Technology, Dynamics and Mission Applications*, Springer–Praxis Series in Space Science and Technology, Springer–Praxis, Berlin, Heidelberg, New York, Chicester, 1999.

[12]Battin, R., *An Introduction to the Mathematics and Methods of Astrodynamics*, AIAA Education Series, American Institute of Aeronautics and Astronautics, Reston, revised ed., 1999.

[13]Dachwald, B., *Low-Thrust Trajectory Optimization and Interplanetary Mission Analysis Using Evolutionary Neurocontrol*, Doctoral thesis, Universität der Bundeswehr München; Fakultät für Luft- und Raumfahrttechnik, 2004.

[14]Dachwald, B., "Optimization of Interplanetary Solar Sailcraft Trajectories Using Evolutionary Neurocontrol," *Journal of Guidance, Control, and Dynamics*, Vol. 27, No. 1, pp. 66–72.

[15]Dachwald, B., "Optimization of Very-Low-Thrust Trajectories Using Evolutionary Neurocontrol," *Acta Astronautica*, Vol. 57, No. 2-8, 2005, pp. 175–185.

[16]Wright, J., "Solar Sailing – Evaluation of Concept and Potential," Tech. rep., Battelle Columbus Laboratories, Columbus, Ohio, March 1976, BMI-NLVP-TM-74-3.

[17]Wright, J. and Warmke, J., "Solar Sail Mission Applications," AIAA/AAS Astrodynamics Conference, San Diego, USA, August 18-20, 1976, AIAA-76-808.

[18]Sauer, C., "A Comparison of Solar Sail and Ion Drive Trajectories for a Halley's Comet Rendezvous Mission," AAS/AIAA Astrodynamics Conference, Jackson, USA, September 1977, 77-104.

[19]Dachwald, B., "Optimal Solar Sail Trajectories for Missions to the Outer Solar System," *Journal of Guidance, Control, and Dynamics*, in press.

[20]Ahrens, T. and Harris, A., "Deflection and Fragmentation of Near-Earth Asteroids," *Hazards Due to Comets and Asteroids*, edited by T. Gehrels, The University of Arizona Press, Tucson, USA, 1994, pp. 897–927.

[21]Gold, R., "SHIELD: A Comprehensive Earth Protection System," A Phase 1 Report to the NASA Institute for Advanced Concepts, NIAC, 1999.

[22]Housen, R. and Holsapple, K., "Impact Cratering on Porous Asteroids," *Icarus*, Vol. 163, 203, pp. 102–119.

[23]Wie, B., "Solar Sailing Kinetic Interceptor (KEI) Mission for Impacting/Deflecting Near-Earth Asteroids," 41st AIAA/ASME/SAE/ASEE Joint Propulsion Conference and Exhibit, Tucson, USA, July 10-14, 2005, AIAA-2005-3725.

[24]Dachwald, B., Seboldt, W., Macdonald, M., Mengali, G., Quarta, A., McInnes, C., Rios-Reyes, L., Scheeres, D., Wie, B., Görlich, M., Lura, F., Diedrich, B., Baturkin, V., Coverstone, V., Leipold, M., and Garbe, G., "Potential Solar Sail Degradation Effects on Trajectory and Attitude Control," AIAA Guidance, Navigation, and Control Conference, San Francisco, USA, August 2005, AIAA-2005-6172.

[25]Dachwald, B., Baturkin, V., Coverstone, V., Diedrich, B., Garbe, G., Görlich, M., Leipold, M., Lura, F., Macdonald, M., McInnes, C., Mengali, G., Quarta, A., Rios-Reyes, L., Scheeres, D., Seboldt, W., and Wie, B., "Potential Effects of Optical Solar Sail Degradation on Trajectory Design," AAS/AIAA Astrodynamics Specialist Conference, Lake Tahoe, USA, August 2005, AAS 05-413.